Journal of Molecular Structure xxx (xxxx) xxx

Contents lists available at ScienceDirect

Journal of Molecular Structure

journal homepage: http://www.elsevier.com/locate/molstruc

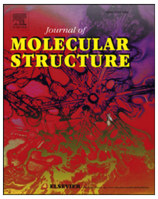

Synthesis, characterization, optical properties, computational characterizations, QTAIM analysis and cyclic voltammetry of new organic dyes for dye-sensitized solar cells

Zahra Agheli, Mehdi Pordel*, Safar Ali Beyramabadi

Department of Chemistry, Mashhad Branch, Islamic Azad University, Mashhad, Iran

ARTICLE INFO

Article history:
Received 10 August 2019
Received in revised form
8 October 2019
Accepted 13 October 2019
Available online xxx

Keywords:
Dye-sensitized solar cells
Purple dyes
3-Nitropyrazolo[1,5-*a*]pyridine
DFT
Cyclic voltammetry
AIM

ABSTRACT

In recent years, dye-sensitized solar cells (DSSCs) have regarded as potential solar cells for the next generation of photovoltaic technologies. Many organic compounds are explored and used in DSSCs to produce low-cost devices and improve the cell efficiency. In this work, three new heterocyclic purple dyes are synthesized from the reaction of 3-nitropyrazolo[1,5-*a*]pyridine with various arylacetonitriles for dye-sensitized solar cells (DSSCs), exhibiting high molar extinction coefficients and a broad absorption range led to the good photovoltaic performance of 6.95–7.18%. Physical spectral, analytical data and optical properties are established the structures of the new dyes. The optimized geometries and relevant frontier orbitals of the dyes are obtained by density functional theory (DFT) at the level of B3LYP/6-311 + G(d,p). Electrostatic potential maps and electron density maps of the dyes were also obtained by atoms in molecules (AIM) analysis. Cyclic voltammetry measurement was performed to evaluate the electrochemical properties of the dyes and reversible oxidation waves were observed for them.

1. Introduction

Dye sensitized solar cells (DSSCs) are considered as the most efficient third-generation solar technology available. They are extensively used in various applications such as rooftop solar collectors. The power production efficiency is around 11%, as compared to thin-film technology cells which are between 5% and 13%, and traditional commercial silicon panels which operate between 12% and 15%.

The sensitized dyes are one of the main components of DSSCs, which correspond to the photo-driven electron pump of the device. Many organic and inorganic compounds have been examined for semiconductor sensitization, such as fluorescent dyes [1], phthalocyanines [2], porphyrins [3], carboxylated derivatives of anthracene [4], chlorophyll derivatives [5], platinum complexes [6,7] and polymeric films [8].

On the other hand, pyrazolopyrimidines are bicyclic ring systems which have recently received considerable attention due to their constructional structure in anticancer agents [9–11]. Among those pyrazolopyrimidine derivatives, pyrazolo[1,5-*a*]pyridines show potent biological effects such as anti-microbial [12], anti-inflammatory [13], anti-tumor [14], anti-fungal [15], anti-tubercular [16] and anti-viral activities [17]. Also, they possess interesting optical properties as dye and fluorescent compounds [18–20]. To the best of our knowledge, no significant study has been done on pyrazolo[1,5-*a*]pyridine derivatives for DSSCs. Herein, three new pyrazolo[1,5-*a*]pyridine dyes were designed and synthesized for dye-sensitized solar cells. The structures of the compounds were confirmed by their physical spectral and analytical data. The density functional theory (DFT) at the level of B3LYP/6-311 + G(d,p) was employed to obtain the optimized geometries and relevant frontier orbitals of the dyes. Furthermore, electrostatic potential maps and electron density maps of the dyes were determined by atoms in molecules (AIM) analysis. Cyclic voltammetry measurement was also used to evaluate the electrochemical properties of the dyes and a reversible oxidation wave was observed for them. The photovoltaic performance parameters of the dyes were elucidated by IPCE spectra and the *I*–*V* curves.

2. Experimental

2.1. Materials and equipment

1-Aminopyridinium iodide, ethyl propiolate and aryl acetonitriles were purchased from Sigma–Aldrich. Compounds **1** (pyrazolo

---

* Corresponding author.
E-mail address: mehdipordel58@mshdiau.ac.ir (M. Pordel).

https://doi.org/10.1016/j.molstruc.2019.127228
0022-2860/© 2019 Elsevier B.V. All rights reserved.

Please cite this article as: Z. Agheli et al., Synthesis, characterization, optical properties, computational characterizations, QTAIM analysis and cyclic voltammetry of new organic dyes for dye-sensitized solar cells, Journal of Molecular Structure, https://doi.org/10.1016/j.molstruc.2019.127228

[1,5-*a*]pyridine) and **2** (3-nitropyrazolo[1,5-*a*]pyridine) were synthesized according to the procedures reported in the literatures [21,22]. Other reagents were purchased from Merck. All solvents were dried according to standard procedures.

Melting points were obtained on an Electrothermaltype-9100 melting-point apparatus. The FT-IR (as KBr discs) spectra were measured on a Tensor 27 spectrometer and only noteworthy absorptions are listed. The ^{13}C NMR (75 MHz), the ^{1}H NMR (300 MHz) and NOESY spectra were recorded on a Bruker Avance DRX-300 spectrometer. Chemical shifts are reported in ppm downfield from TMS as internal standard; coupling constant *J* is given in Hz. The mass spectra were obtained on a Varian Mat, CH-7 at 70 eV. Elemental analysis was performed on a Thermo Finnigan Flash EA microanalyzer. Absorption and fluorescence spectra were recorded on Varian 50-bio UV—Visible spectrophotometer and Varian Cary Eclipse spectrofluorophotometer. UV—vis scans were obtained from 200 to 800 nm. Cyclic voltammograms were recorded on a 797 V A Computrace Metrohm. Tetrabutylammonium perchlorate (TBAP) was utilized used as the supporting electrolyte and a platinum wire served as a counter electrode and Ag/AgCl (KCl 3 M) was used as a reference electrode. The concentrations used to obtain each voltammogram are given in the corresponding figure caption. Voltage-Current analyses were done using an EIS-26H model of Potentiostat-Galvanostat at ±5 V.

2.2. General procedure for the synthesis of 4a—c

Compounds **2** (1.63 g, 10 mmol) and arylacetonitriles **2a**—***c*** (12 mmol) were added with stirring to a solution of KOH (20 g, 357 mmol) in MeOH (30 mL). The mixture was refluxed with stirring for 3 h, and then poured into water. The precipitate was collected by filtration, after neutralization with dilute HCl solution. Then, it was washed with water and then air dried to give crude **4a**—**c**. More purification was obtained by crystallization from acetone.

2.2.1. (2E,3E)-2-(Cyano(phenyl)methylene)-3-(hydroxyimino)-2,3-dihydropyrazolo [1,5-a]pyridin-8-ium-1-ide (4a)

Compound **4a** was obtained as purple powder, yield (79%), mp 210—212 °C; ^{1}H NMR (DMSO-d_6) δ 6.56 (t, $J = 7.5$ Hz, 1H, Ar H), 7.09 (d, $J = 8.7$ Hz, 1H, Ar H), 7.25 (t, $J = 7.5$ Hz, 1H, Ar H), 7.43 (t, $J = 8.3$ Hz, 2H, Ar H), 7.58—7.64 (m, 1H, Ar H), 8.16 (d, $J = 8.3$ Hz, 2H, Ar H), 9.01 (d, $J = 6.9$ Hz, 1H, Ar H), 13.44 (br s, 1H, OH); ^{13}C NMR (DMSO-d_6) δ 118.3, 119.7, 125.2, 126.4, 128.6, 128.9, 130.3, 130.8, 133.6, 134.8, 136.3, 145.7, 156.4; IR (KBr): 3455 cm^{-1} (OH), 2190 cm^{-1} (CN). MS (*m*/*z*) 262 (M$^+$). Anal. Calcd for $C_{15}H_{10}N_4O$ (262.3): C, 68.69; H, 3.84; N, 21.36. Found: C, 69.02; H, 3.86; N, 21.12.

2.2.2. (2E,3E)-2-((4-Chlorophenyl)(cyano)methylene)-3-(hydroxyimino)-2,3-dihydropyrazolo [1,5-a]pyridin-8-ium-1-ide (4b)

Compound **4b** was obtained as purple powder, yield (83%), mp 228—230 °C; ^{1}H NMR (DMSO-d_6) δ 6.63 (t, $J = 7.5$ Hz, 1H, Ar H), 7.12 (d, $J = 8.7$ Hz, 1H, Ar H), 7.46 (d, $J = 8.6$ Hz, 2H, Ar H), 7.67 (t, $J = 7.5$ Hz, 1H, Ar H), 8.20 (d, $J = 8.6$ Hz, 2H, Ar H), 9.05 (d, $J = 6.9$ Hz, 1H, Ar H), 13.53 (br s, 1H, OH); ^{13}C NMR (DMSO-d_6) δ 117.8, 118.5, 125.3, 126.0, 128.2, 129.3, 130.9, 131.3, 133.4, 134.5, 137.8, 145.0, 159.8; IR (KBr): 3453 cm^{-1} (OH), 2199 cm^{-1} (CN). MS (*m*/*z*) 296 (M$^+$), 298 (M$^+$ + 2). Anal. Calcd for $C_{15}H_9ClN_4O$ (296.7): C, 60.72; H, 3.06; N, 18.88. Found: C, 61.08; H, 3.09; N, 18.59.

2.2.3. (2E,3E)-2-(Cyano(4-methoxyphenyl)methylene)-3-(hydroxyimino)-2,3-dihydropyrazolo [1,5-a]pyridin-8-ium-1-ide (4c)

Compound **4c** was obtained as purple powder, yield (84%), mp 199—201 °C; ^{1}H NMR (DMSO-d_6) δ 3.83 (s, 3H, OCH_3), 6.65 (t, $J = 7.5$ Hz, 1H, Ar H), 7.15 (d, $J = 8.7$ Hz, 1H, Ar H), 7.31 (d, $J = 8.4$ Hz, 2H, Ar H), 7.65 (t, $J = 7.5$ Hz, 1H, Ar H), 8.19 (d, $J = 8.4$ Hz, 2H, Ar H), 8.99 (d, $J = 6.9$ Hz, 1H, Ar H), 13.49 (br s, 1H, OH); ^{13}C NMR (DMSO-d_6) δ 57.3, 117.3, 117.9, 125.1, 126.6, 127.7, 129.4, 131.5, 132.8, 134.7, 134.9, 136.2, 145.7, 157.9; IR (KBr): 3452 cm^{-1} (OH), 2193 cm^{-1} (CN). MS (*m*/*z*) 292 (M$^+$). Anal. Calcd for $C_{16}H_{12}N_4O_2$ (292.3): C, 65.75; H, 4.14; N, 19.17. Found: C, 66.11; H, 4.16; N, 18.98.

2.3. Computational details

All of the DFT method calculations have been performed by using the B3LYP functional [23] and 6-311 + G(d,p) basis sets. The Gaussian 03 program [24] was used. Geometries of the investigated species were fully optimized, which were used for the complementary calculations. The optimized geometries don't show any imaginary frequency. In the frequency calculations, the DFT-calculated vibrational frequencies are higher than the experimental ones. Since, the calculated vibrational frequencies were improved by applying the scale factor of 0.9614 [25]. The gauge-including atomic orbital (GIAO) method [26] was used to predict the ^{1}H NMR chemical shifts of the investigated compounds with respect to the tetramethylsilane (TMS) in DMSO-d_6 as the solvent. Also, the NBO analysis was performed to identify highest-occupied-molecular orbital (HOMO) and the lowest-unoccupied-molecular orbital (LUMO) frontier orbitals. The Chemcraft 1.7 program was employed for visualization of structures [27].

In addition to the DFT calculations, the QTAIM was employed to characterize important bonds and rings. The QTAIM calculations have been performed using the AIMALL package [28]. The QTAIM calculations are based on the topological analysis of the electron density, ρ(r) [29]. On the other hands, the kinetic energy density (G_b), the potential energy density (V_b), the total energy density (H_b), the electron density (ρ) and its Laplacian ($\nabla^2\rho$) at a bond critical point (BCP) are related to the electron density. These quantities are used to realize nature of the bonds.

2.4. Photoelectrochemical measurements

To investigate the properties of the solar cells which made by our dyes (DSSCs), we used titanium dioxide (TiO_2) nanoparticles in rutile phase (p-25), (I^-/I_3^-) standard electrolyte, acetic acid (99% sigma Aldrich), ethanol (99% Merck) and FTO glasses.

For DSSCs fabrication, FTO glasses cleaned 3 times with deionized water, acetone and ethanol in ultrasonic bath, and their conductive side was determined by Ohm meter. Then TiO_2 paste was deposited on one of them by Doctor Blade's method [30]. TiO_2 paste was prepared using TiO_2 nano powder (2 g) which were grinded in mortar by adding three drops acetic acid.

During grinding process two another drops of acetic acid were added in order to making colloidal paste with fluid and uniform consistency. In the next step, 0.2 g polyethylene glycol (2000) and deionized water were added and mixed with the paste completely to make that sticky. This process causes paste to stick better to the slide. After a while, when the paste was dried to some extent, the slides were heated in oven in 450 °C for 30 min. The dried slides were placed in dyes for 20 h.

Counter electrodes were fabricated depositing Pt paste on FTO. These deposited FTO were connected to those which TiO_2 paste was deposited on and completely were sealed. Then electrolyte was

Please cite this article as: Z. Agheli et al., Synthesis, characterization, optical properties, computational characterizations, QTAIM analysis and cyclic voltammetry of new organic dyes for dye-sensitized solar cells, Journal of Molecular Structure, https://doi.org/10.1016/j.molstruc.2019.127228

injected to empty space between two electrodes on effective surface (0.25 cm^2).

A solar simulator system under 1.5 A M and intensity of 100 mW/cm^2 (SIM 1000, Sharif solar) was applied for investigating of photovoltaic characteristics including short circuit current, open circuit voltage, fill factor, and cells efficiency.

3. Results and discussion

The precursor of 3-nitropyrazolo[1,5-*a*]pyridine (**2**) was synthesized according to reported procedures [21,22]. Reaction of 1-aminopyridinium iodide with ethyl propiolate gave ethyl pyrazolo[1,5-*a*]pyridine-3-carboxylate (Scheme 1). Pyrazolo[1,5-*a*]pyridine (**1**) was obtained when ethyl pyrazolo[1,5-*a*]pyridine-3-carboxylate was hydrolyzed in aqueous KOH and MeOH and then decarboxylation by heating in HI [21]. Nitration of compound **1** in HNO_3/H_2SO_4 led to the formation of 3-nitropyrazolo[1,5-*a*]pyridine (**2**) in good yield [22]. Finally, the new heterocyclic purple dyes **4a**–**c** were synthesized from the reaction of compound **2** with aryl acetonitriles **3a**–**c** in excellent yields (Scheme 1).

A tentative mechanism to clarify the formation of dyes **4a**–**c** is depicted in Scheme 2. As shown, the new dyes **4a**–**c** are obtained by attack of the deprotonated form of compounds **3a**–**c** on 3-nitropyrazolo[1,5-*a*]pyridine (**2**) and then subsequent protonation.

Physical spectral (^1H, ^{13}C NMR, FT-IR spectra) and analytical data confirm the structure of new dyes **4a**–**c**. For example, there is an exchangeable peak at δ 13.53 ppm attributed to OH group proton in the ^1H NMR spectrum of compound **4b.** Moreover, in the ^{13}C NMR spectrum of dye **4b**, there are 13 different carbon atoms. A weak absorption band at 2199 cm^{-1} and a broad absorption band at 3453 cm^{-1} assignable to CN and OH groups are observed in the FT-IR spectrum of the compound **4b,** respectively. Analytical data and the mass spectrum are also further confirmed the structure of dye **4b**. Furthermore, as can be seen in Scheme 2, no cross-peak between the OH proton (δ 13.53, br s) and the aromatic protons is observed in the data from NOESY experiment of dye **4b** which confirms the *2E, 3E* configuration of the new dyes (Scheme 3).

The DFT method calculations by using the B3LYP functional and 6-311 + G(d,p) basis sets are used to deduce the configuration of new dyes **4a**–**c.** Each of the dyes **4a**–**c** has four different isomers. For example, the DFT-optimized geometries for four isomers of dye **4b** are shown in Fig. 1 with labeling of their atoms. These four isomers are named as the **4b1**, **4b2**, **4b3** and **4b4** species. The calculated relative energies of four isomers are listed in Table 1. As seen, the **4b1** (*2E, 3E*) isomer is the most stable isomer in MeOH solution of dye **4b**. Similar to dye **4b**, the **4a1** and **4c1** isomers are the most stable isomers in methanol solution of dyes **4a** and **4c**, respectively. Optimized geometries of the **4a1** and **4c1** isomers of dyes **4a** and **4c** are shown in Fig. 2. As seen in Figs. 1 and 2, all the **4a1**, **4b1** and **4c1** species involve the O1H5···N4 intramolecular-H bond, which increases stability of these isomers rather than the other isomers of dyes **4a**–**c.**

Selected structural parameters of the dyes **4a**–**c** are gathered in Table 2. As seen, their structures are roughly planar, but pyrazolo[1,5-*a*]pyridine and benzene rings make a dihedral of about 30° to each other. The C8–C9–N4 moiety makes a dihedral angle about 20 and 10° with pyrazolo[1,5-*a*]pyridine and benzene rings, respectively.

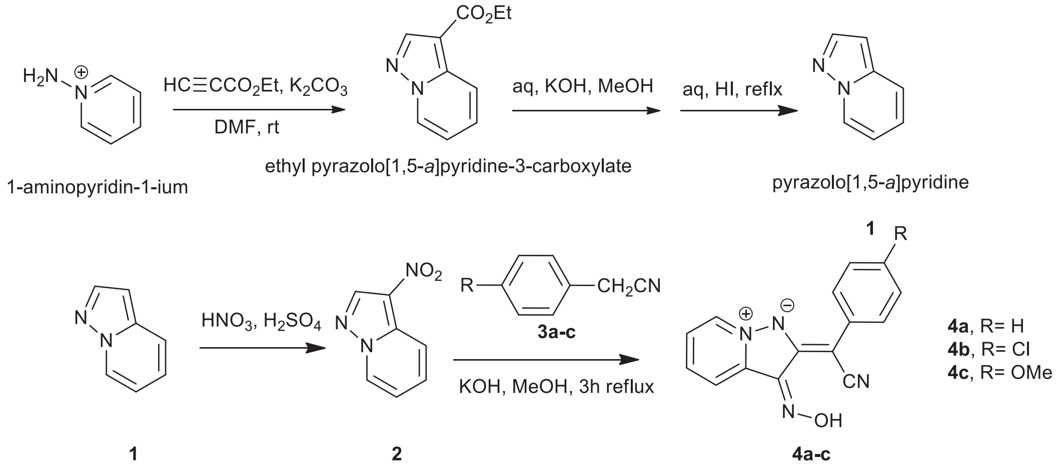

Scheme 1. Synthesis of new purple dyes **4a**–**c.**

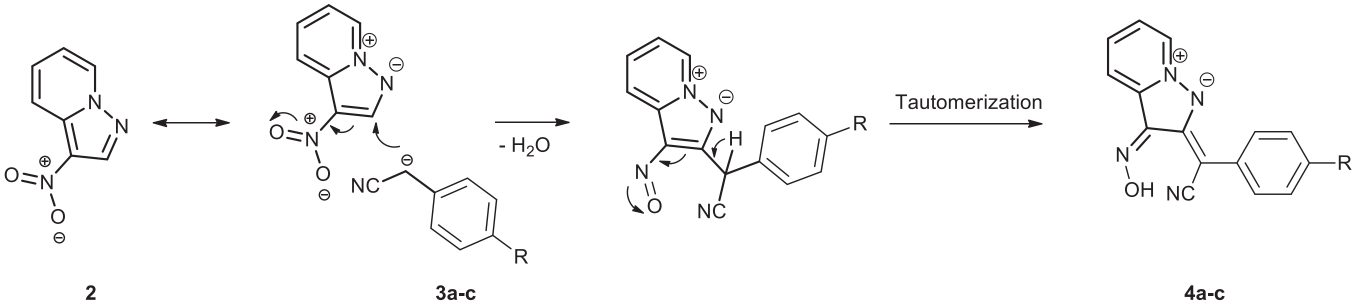

Scheme 2. A proposed mechanism to explain the formation of dyes **4a**–**c**.

Please cite this article as: Z. Agheli et al., Synthesis, characterization, optical properties, computational characterizations, QTAIM analysis and cyclic voltammetry of new organic dyes for dye-sensitized solar cells, Journal of Molecular Structure, https://doi.org/10.1016/j.molstruc.2019.127228

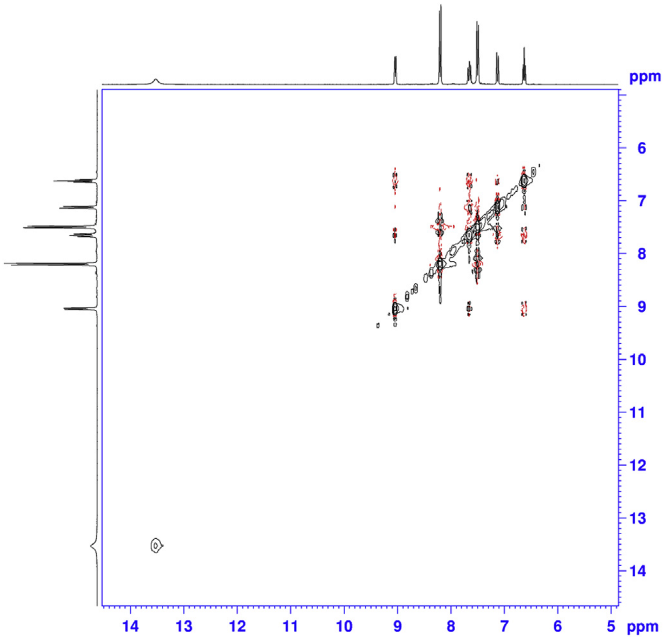

Scheme 3. NOESY spectrum of dye **4b**.

3.1. NMR spectra

Herein, the NMR spectra of the **4a**–**c** compounds have been identified by using the DFT calculations. The experimental and DFT-computed ^{1}H NMR chemical shifts (δ) of the compounds are listed in Table 3. The atom positions of the **4a1**, 4**b1** and **4c1** species are numbered as in Figs. 1 and 2.

As seen in Table 3, there is good agreement between the experimental and DFT-computed chemical shifts, approving validity of 4**a1**, **4b1** and **4c1** geometry for the optimized geometries of the compounds **4a**–**c** respectively. Especially, a signal at 12.74, 12.90 and 12.63 ppm for **4a**, **4b** and 4**c** compounds, respectively, is related to the NOH moiety, confirm suitability of the **4a1**, **4b1** and 4**c1** optimized geometries.

3.2. Vibrational spectroscopy

Comparing the experimental and DFT-calculated vibrational frequencies for the species **4a1**, **4b1** and 4**c1**, important IR vibrational bands of the investigated compounds have been assigned. The obtained results are gathered in Table 4.

In the 3600-2500 cm^{-1} spectral region of the IR spectra, overlapping of the O–H, N–H, S–H and C–H stretching vibrations causes to broad bands [31–34]. Observed bands of this region have been assigned theoretically. The obtained results are given in Table 4. As seen, the most intensive band is related to the stretching vibrations of the O1–H5 bond.

3.3. NBO analysis

Many characters of the chemical compounds such as the frontier orbitals, energy gap, stability, electronic charge transfers, the bond order, the intra- and intermolecular bonding interactions can be explored by employing the NBO analysis [32–37]. For example, the 3D-distribution maps of the HOMO and the LUMO frontier orbitals of the species 4**b1** are shown in Fig. 3. As seen, both of the HOMO orbital is mainly localized on the benzene ring; but the LUMO orbital is mainly localized on the pyrazolo[1,5-*a*]pyridine ring.

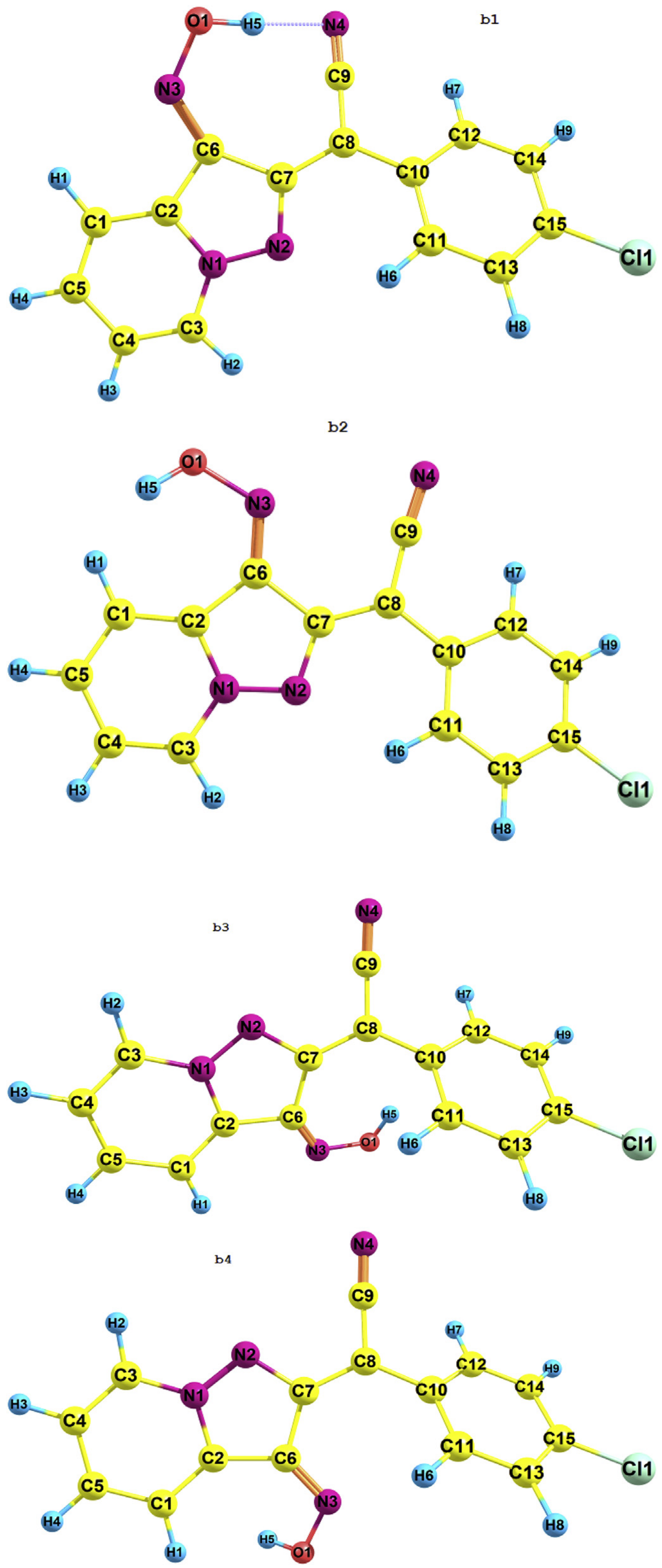

Fig. 1. Optimized geometries of the four possible isomers (**4b1**-**4b4**) of dye **4b** together with their labeling.

The energy difference between the HOMO and LUMO frontier orbitals is named as the energy gap, which has an essential role in many characters of the chemical compounds such as the electron

Please cite this article as: Z. Agheli et al., Synthesis, characterization, optical properties, computational characterizations, QTAIM analysis and cyclic voltammetry of new organic dyes for dye-sensitized solar cells, Journal of Molecular Structure, https://doi.org/10.1016/j.molstruc.2019.127228

Table 1
The relative energies (kJ.mol^{-1}) of the investigated species **4a**–**c**.

Species	relative energies	Species	relative energies	Species	relative energies
4a1	0.0	4b1	0.0	4c1	0.0
4a2	23.63	4b2	23.10	4c2	22.04
4a3	7.88	4b3	10.97	4c3	6.73
4a4	30.15	4b4	30.36	4c4	26.92

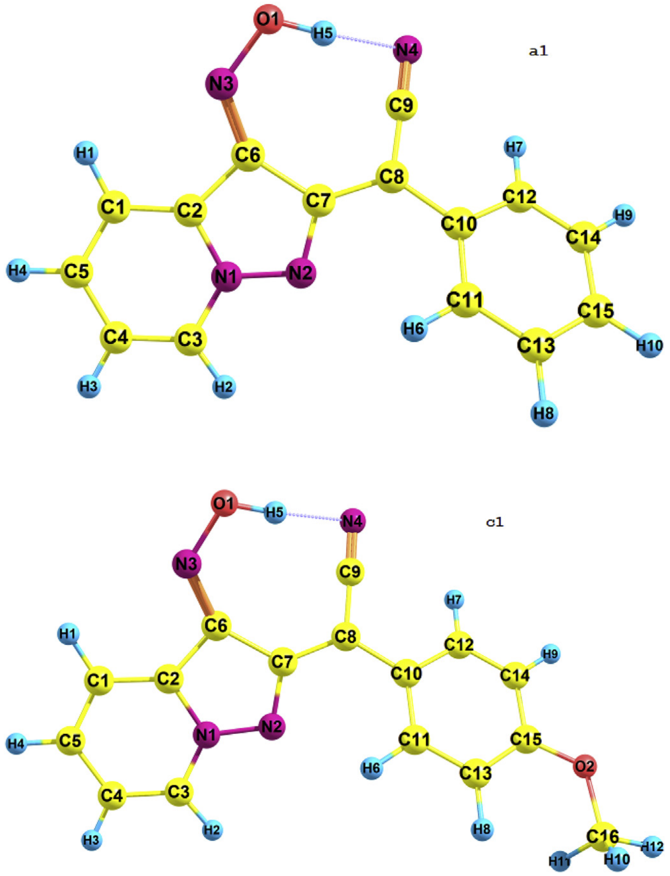

Fig. 2. Optimized geometries of the 4**a1** and **4c1** isomers of dyes **4a** and **4c**.

transitions and the photochemical reactions. The calculated energy gaps for the compounds **4a**–**c** are 2.38, 2.35 and 2.25 respectively.

3.3.1. AIM analysis

Based on the AIM analysis, the nature of important intramolecular bonds as well as the electronic density ($\rho(r)$) of the aromatic rings have been evaluated for all of the **4a1**-**c1** species. The calculated values of $\rho(r)$, $\nabla^2\rho(r), H_b, G_b, V_b$ and $-G_b/V_b$ at BCP are gathered in Table 5. Optimized geometry for each of the **4a1**, **4b1** and **4c1** species involves two intramolecular H-bonds, O1–H5···N4 and C11–H6···N2. As seen in Table 5, for both of these H-bonds $\nabla^2\rho(r)$ and H_b are positive, confirming weakness of these H-bonds. On the other hands, the $-G_b/V_b$ value is greater than 1, which is correspond to the noncovalent property of these bonds [38]. Also, the hydrogen bond energies can be calculated by $E_{HB} = {}^{1}/2V_b$ Ref. [39]. For the **4a1** species, the calculated E_{HB} values for the O1–H5–N4 and C11–H6–N2 H-bonds are −23.76 and −47.43H, respectively. These values are −23.76 and −51.82H for the **4b1** species, −24.06 and −48.93H for the **4c1** species, respectively. For example, the molecular graph of the species **4b1** is shown in Fig. 4, where small green and red spheres correspond to the bond critical points (BCPs) and the ring critical points (RCPs), respectively.

Considering the H5–N4 and H6–N2 H-bonds, there are five rings in structure of the investigated compounds (Fig. 4). The $\rho(r)$ values of these rings have been computed and reported in Table 6. As seen, the pyrazole ring involves the highest electron density in structure of all investigated compounds.

3.4. Photophysical properties of compounds 4a–c

The absorption spectra of compounds **4a**–**c** were investigated by UV–Vis spectroscopy in 10^{-5} M MeOH solution, in the wavelength range of 200–800 nm (Fig. 5). Table 7 shows numerical spectral data of dyes **4a-c**. Values of extinction coefficient (ε) were obtained as the slope of the plot of absorbance *vs* concentration. Absorption maximums of dyes **4a-c** can be observed at 325 and 530 nm in the UV–Vis spectra of the dyes. Intramolecular charge transfer (ICT) states [40] from OH group and endocyclic N2 (as donor sites) to CN (C≡N and $-C{=}N^{+}$) group (as acceptor moiety) can be proposed for the appearance of the signals in the visible region of the investigated dyes **4a**–**c** (see Fig. 6).

As depicted in Fig. 5, a relatively sharp peak at 325 nm can be considered as π- π^* transitions (donor endocyclic nitrogen to the acceptor CN (C≡N and $-C{=}N^{+}$) group) and a broad band at 530 nm can be attributed to n- π^* transitions from the donor OH group to the acceptor CN group.

The solvatochromic properties of dyes **4a-c** were studied and summarized in Table 7. The obtained results revealed that the visible absorption spectra of the dyes undergo a relatively modest red shift in polar solvents. Increasing the solvent polarity stabilizes the ICT excited-state molecule relative to the ground-state molecule and leads to the observed red shift of the absorption maximum as the experimentally observed result (Table 7). For example, in the absorption spectra of dye **4a**, λ_{abs} shifts from 530 to 515 nm as the solvent changes from methanol to n-hexane (Table 7).

3.5. Electrochemical properties

The electrochemical properties of the dyes **4a**–**c** were examined to gain more quantitative insight into the redox properties of the dyes. Cyclic voltammetry was employed in the presence of tetrabutylammonium perchlorate (TBAP) as the supporting electrolyte, using Pt working and counter electrodes and Ag/AgCl as reference electrode in DMF as the solvent. The potentials were referenced to ferrocene/ferrocenium (Fc/Fc^{+}) as the internal reference.

For example, as seen in Fig. 7, cyclic voltammogram of dye **4c** (−1 to +1 V) revealed an oxidation wave with an anodic peak potential of −0.112 V and a cathodic peak potential of −0.210 V versus SCE ($i_{pa}/i_{pc} \approx 1$). The observed peak separation for the reversible waves was larger than the value of 59/n mV expected for a reversible system, suggesting that the redox couple has a quasi-reversible behavior [41]. Scan rate studies of dye **4c** showed that the anodic and cathodic peak currents (i_{pa}, i_{pc}) of the oxidation wave were proportional to the square root of the scan rate ($\nu^{1/2}$)

Please cite this article as: Z. Agheli et al., Synthesis, characterization, optical properties, computational characterizations, QTAIM analysis and cyclic voltammetry of new organic dyes for dye-sensitized solar cells, Journal of Molecular Structure, https://doi.org/10.1016/j.molstruc.2019.127228

Table 2
Selected structural parameters of the *2E, 3E* isomer of the investigated compounds.

	Species		
	4a1	4b1	4c1
Bond length (pm)			
C1—C2	138.6	138.6	138.6
C2—N1	136.7	136.7	136.8
N1—N2	135.4	135.6	135.2
N2—C7	135.9	135.8	136.2
C7—C6	150.4	150.4	150.2
C6—N3	130.0	130.0	130.0
N3—O1	134.2	134.1	134.5
O1—H5	98.2	98.2	98.1
H5···N4	196.3	196.2	196.9
C7—C8	140.0	140.1	140.0
C8—C9	141.0	141.0	141.1
C9—N4	116.4	116.4	116.4
C8—C10	147.6	147.4	147.2
C10—C11	140.8	140.9	140.5
C15—H10	108.4	–	–
C15—Cl	–	175.8	–
C15—O2	–	–	136.2
O2—C16	–	–	142.2
Angle (°)			
C5—C1—C2	118.8	118.8	118.9
C4—C3—N1	118.9	118.9	118.9
C3—N1—N2	123.1	123.1	123.2
N1—N2—C7	106.9	106.9	106.8
N2—C7—C6	109.0	109.0	109.0
C7—C6—N3	140.6	140.8	140.7
C6—N3—O1	123.6	123.7	123.4
N3—O1—H5	113.6	113.7	113.5
O1—H5—N4	163.9	163.7	164.2
N2—C7—C8	121.8	121.8	121.6
C7—C8—C9	116.9	116.8	116.8
C8—C9—N4	178.3	178.4	178.3
C7—C8—C10	126.3	126.5	126.6
C8—C10—C11	122.7	123.0	123.2
C10—C11—C13	120.7	121.2	121.6
C13—C15—Cl	–	119.7	–
C13—C15—O2	–	–	124.8
C15—O2—C16	–	–	118.7
Dihedral angle (°)			
C1—C5—C4—C3	0.1	0.1	0.1
C4—C3— N1—N2	−179.2	−179.2	−179.3
N1—N2—C7—C6	4.8	4.6	4.9
N2—C7—C6—N3	160.8	161.1	161.0
C7—C6—N3—O1	7.6	7.5	7.2
C6—N3—O1—H5	18.7	18.2	19.1
N2—C7—C8—C9	162.1	162.3	162.3
C7—C8—C9—N4	−36.4	−42.1	−48.3
C10—C8—C9—N4	137.8	132.3	126.2
C9—C8—C10—C11	166.4	170.4	169.3
N2—C7—C8—C10	−11.5	−11.4	−11.4
C7—C8—C10—C11	−20.0	−15.8	−17.0
C8—C10—C11—C13	−177.9	−178.2	−178.1
C10—C11—C13—C15	−0.3	−0.3	−0.2
C11—C13—C15—Cl	–	−179.6	–
C11—C13—C15—O2	–	–	−179.8
C13—C15—O2—C16	–	–	−0.8

Table 3
Experimental and DFT-calculated ^{1}H NMR chemical shifts of the investigated compounds in DMSO solution, δ)ppm(.

Species	Experimental			Theoretical		
	4a	4b	4c	4a1	4b1	4c1
Atom position						
H1	7.09	7.12	7.15	7.07	7.07	7.02
H2	9.01	9.05	8.99	9.15	9.17	9.11
H3	6.56	6.63	6.65	7.18	7.23	7.17
H4	7.25	7.67	7.65	7.18	7.23	7.12
H5	13.44	13.53	13.49	12.74	12.90	12.63
H6	8.16	7.46	7.31	8.12	7.92	7.56
H7	8.16	7.46	7.31	8.07	7.70	7.47
H8	7.43	8.20	8.19	7.44	8.36	7.97
H9	7.43	8.20	8.19	7.44	8.49	8.17
H10	7.58–7.64	–	3.83	7.29	–	3.62
H11	–	–	3.83	–	–	3.62
H12	–	–	3.83	–	–	4.01

indicating diffusion control (Fig. 8). Cyclic voltammetric data of dyes **4a**—**c** were summarized in Table 8. The relatively small difference of ΔEP (mV) in dyes **4a**—**c** (Table 8) show that the main reason for observation of the waves in cyclic voltammogram of the dyes is the presence of donor sites (OH group and endocyclic N2) and acceptor moiety (CN group) and the substituent in dyes **4a**—**c** do not have much effect in this case.

3.6. *Photovoltaic properties*

Experimental details of the photovoltaic measurements can be found in experimental section. The IPCE spectra and the *I*—*V* curves are depicted in Fig. 9. The photovoltaic performance parameters (a short circuit photocurrent density (J_{sc}), an open-circuit photovoltage (V_{oc}), a fill factor (ff) and a solar energy-to-electricity conversion yield (η)) are collected in Table 9. The peak IPCE was found to be 64% at 505 nm for **4a** and 67% at 500 nm for **4b**, in contrast to 72% at 500 nm for **4c** based devices. The *I*—*V* curves show that the J_{sc} and η values are 14.92 mA cm^{-2} and 6.95%, 16.62 mA cm^{-2} and 7.06%, 17.60 mA cm^{-2} and 7.18% for **4a**—**c**, respectively. The high photovoltaic performances of DSSCs based on dyes **4a**—**c** are attributed to the high electron-injection efficiency due to the high LUMO level and the faster charge recombination due to the BODIPY core, leading to the low Jsc and Voc values, respectively.

4. Conclusions

New heterocyclic purple dyes were obtained from the reaction of 3-nitropyrazolo[1,5-*a*]pyridine with arylacetonitriles under basic condition. The structure of the dyes was confirmed by physical spectral and analytical data. The data obtained from NOESY experiment revealed that the configuration of the dyes is *2E,3E*. The DFT method calculations by using the B3LYP functional and 6-311 + G(d,p) basis sets were used to approve the configuration of the dyes. There was a good agreement between the experimental

Please cite this article as: Z. Agheli et al., Synthesis, characterization, optical properties, computational characterizations, QTAIM analysis and cyclic voltammetry of new organic dyes for dye-sensitized solar cells, Journal of Molecular Structure, https://doi.org/10.1016/j.molstruc.2019.127228

Table 4
Selected experimental and the DFT-computed IR vibrational frequencies (cm^{-1}) of the investigated compounds. (Intensity is in term of $km.mol^{-1}$).

4a1			4b1			4c1			Vibrational assignment
Exp.	Calculated		Exp.	Calculated		Exp.	Calculated		
	Freq.	Intensity		Freq.	Intensity		Freq.	Intensity	
–	–	–	–	–	–	1440	1446	53	δ_{sci}(methyl group)
1470	1465	24	1455	1462	92	1475	1479	68	υ(C–C) of the benzene ring
1535	1519	168	1515	1517	169	1510	1516	146	υ(C6–N3)
1553	1547	22	1573	1563	43	1590	1581	274	υ(C–C) of the benzene ring
1607	1600	34	1595	1600	30	1596	1600	30	υ(C–C) of the pyridine ring
2174	2165	217	2174	2167	210	2174	2167	229	υ(C9–N4)
–	–	–	–	–	–	2895	2890	74	υ_{sym}(C–H) of the methyl group
–	–	–	–	–	–	2935	2947	36	υ_{asym}(C–H) of the methyl group
3060–3080	3041–3060	15	3073–3089	3061–3075	3	3065–3079	3057–3076	13	υ_{asym}(C–H) of the aromatic rings
3095–3125	3068–3116	24	3100–3129	3087–3116	13	3095–3124	3085–3116	7	υ_{sym}(C–H) of the aromatic rings
3410	3337	47	3430	3337	47	3455	3352	42	υ(O1–H5)

and DFT-computed chemical shifts and IR vibrational frequencies. Moreover, AIM analysis established that the pyrazole ring involves the highest electron density in structure of the compounds. Photophysical properties of the dyes were characterized by UV–Vis spectroscopy and ICT states from donor sites to acceptor moiety was proposed for the appearance of the signals in the visible region of the dyes. Cyclic voltammetry measurement was performed to evaluate the electrochemical properties of the dyes and a reversible oxidation wave was observed for them. The IPCE spectra and the *I–V* curves of the dyes were obtained and the photovoltaic performance of 6.95–7.18% was observed. To further increase of

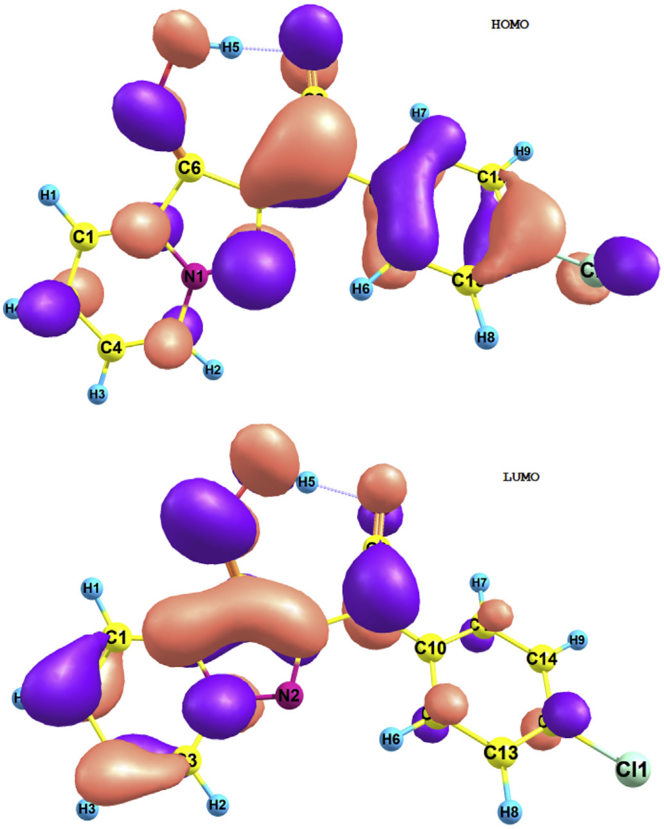

Fig. 3. The HOMO and LUMO frontier orbitals of the species **4b**.

Table 5
Important topological parameters of the **4a1**, **4b1** and **4c1** species in a.u.

Bond	ρ(r)	$\nabla^2\rho$	V_b	G_b	H	$-G_b/V_b$
4a1						
O1–H5	0.345802	−2.40724	−0.7379	0.068043	−0.66985	0.092212
H5···N4	0.030848	0.090805	−0.02104	0.021871	0.000831	1.039496
C11–H6	0.288518	−1.0143	−0.3269	0.036663	−0.29024	0.112154
N2···H6	0.016949	0.063666	−0.01054	0.013229	0.002688	1.255004
4b1						
O1–H5	0.345867	−2.40849	−0.73808	0.067977	−0.6701	0.092100
H5···N4	0.030854	0.090922	−0.02104	0.021887	0.000844	1.040108
C11–H6	0.287679	−1.00738	−0.32651	0.037332	−0.28918	0.114337
N2···H6	0.015708	0.058774	−0.00965	0.012171	0.002523	1.261505
4c1						
O1–H5	0.34697	−2.41546	−0.74067	0.0684	−0.67227	0.092349
H5···N4	0.030544	0.090325	−0.02078	0.02168	0.000901	1.043361
C11–H6	0.288291	−1.01239	−0.32684	0.036872	−0.28997	0.112813
N2···H6	0.016515	0.061892	−0.01022	0.012846	0.002627	1.257070

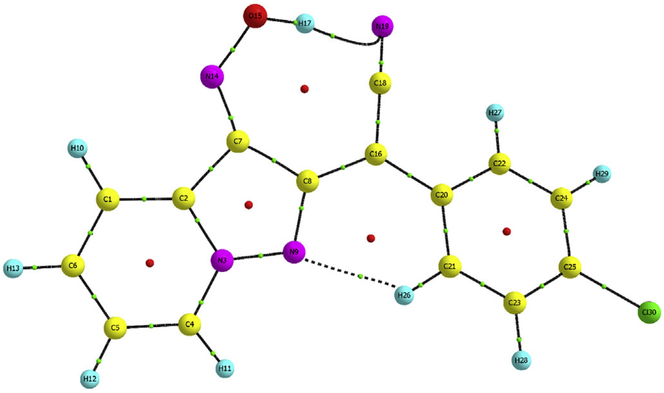

Fig. 4. The QTAIM molecular graphs of the species **4b1**.

Please cite this article as: Z. Agheli et al., Synthesis, characterization, optical properties, computational characterizations, QTAIM analysis and cyclic voltammetry of new organic dyes for dye-sensitized solar cells, Journal of Molecular Structure, https://doi.org/10.1016/j.molstruc.2019.127228

Table 6
The calculated (ρ(r) for aromatic rings in structure of the species **4a1**, **4b1** and **4c1** (in term of C.Bobhr^{-3}).

Member of the ring	Number of atoms	ρ(r)		
		4a1	4b1	4c1
C1–C2–N1–C3–C4–C5	6	+0.022404	+0.022423	+0.022369
C2–N1–N2–C7–C6	5	+0.047429	+0.047400	+0.047433
C6–C7–C8–C9–N4–H5–O1–N3	8	+0.008401	+0.008375	+0.008376
N2–C7–C8–C10–C11–H6	6	+0.010230	+0.010345	+0.010286
C10–C11–C13–C15–C14–C12	6	+0.021538	+0.021533	+0.021299

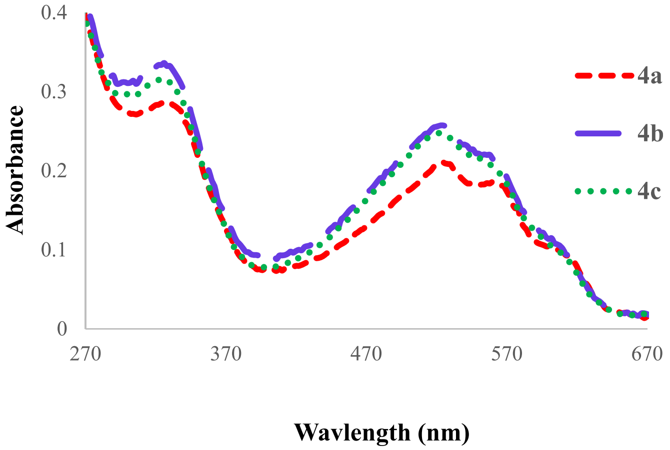

Fig. 5. Visible absorption (10^{-5} mol L^{-1}) of dyes **4a–c** in MeOH.

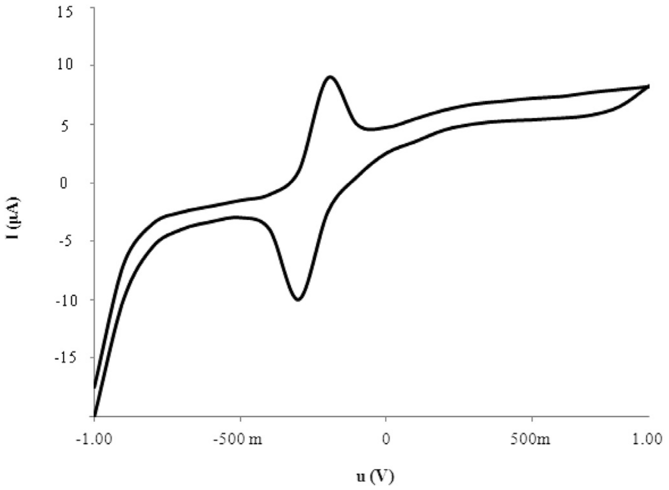

Fig. 7. Cyclic voltammogram of dye **4c** in DMF (10^{-4} M) at scan rate 100 mV/s.

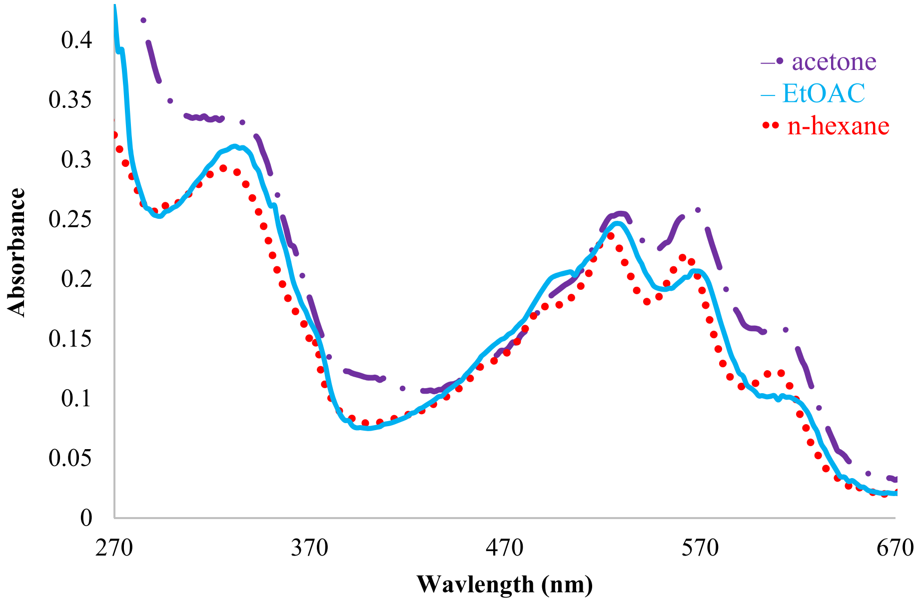

Fig. 6. Visible absorption spectra of compound **4a** in some solvents.

Table 7
Spectroscopic data of dyes **4a–c** in different solvents at 298 K.

Dye Solvent	4a λ_{abs} (nm)[a]	4a $\varepsilon \times 10^{-3}$ [(mol L^{-1})$^{-1}$ cm^{-1}][b]	4b λ_{abs} (nm)	4b $\varepsilon \times 10^{-4}$ [L mol^{-1} cm^{-1}]	4c λ_{abs} (nm)	4c $\varepsilon \times 10^{-4}$ [L mol^{-1} cm^{-1}]
MeOH	325, 530	28.0	320, 530	31.0	320, 530	30.3
Acetone	320, 525, 560	26.0	315, 525	29.5	315, 525	30.5
EtOAc	315, 525	25.5	315, 520	27.0	315, 520	27.5
n-hexane	305, 515	20.0	305, 515	21.1	305, 515	20.7

[a] Wavelengths of maximum absorbance (λ_{abs}).
[b] Extinction coefficient.

Please cite this article as: Z. Agheli et al., Synthesis, characterization, optical properties, computational characterizations, QTAIM analysis and cyclic voltammetry of new organic dyes for dye-sensitized solar cells, Journal of Molecular Structure, https://doi.org/10.1016/j.molstruc.2019.127228

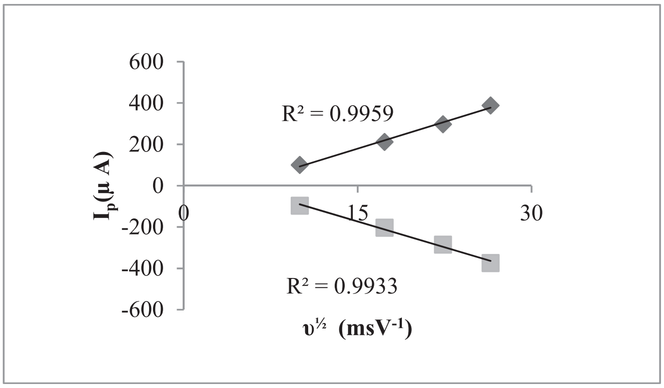

Fig. 8. Plots of anodic and cathodic peak currents *vs* $\upsilon^{1/2}$.

Table 8
Cyclic voltammetric data of dyes **4a**–**c** in scan rates 100 mV/s.

Comp.	Epa (mV)	Epc (mV)	ΔEP (mV)
Ferrocene	556	469	87
4a	−98	−187	89
4b	−105	−197	92
4c	−112	−210	98

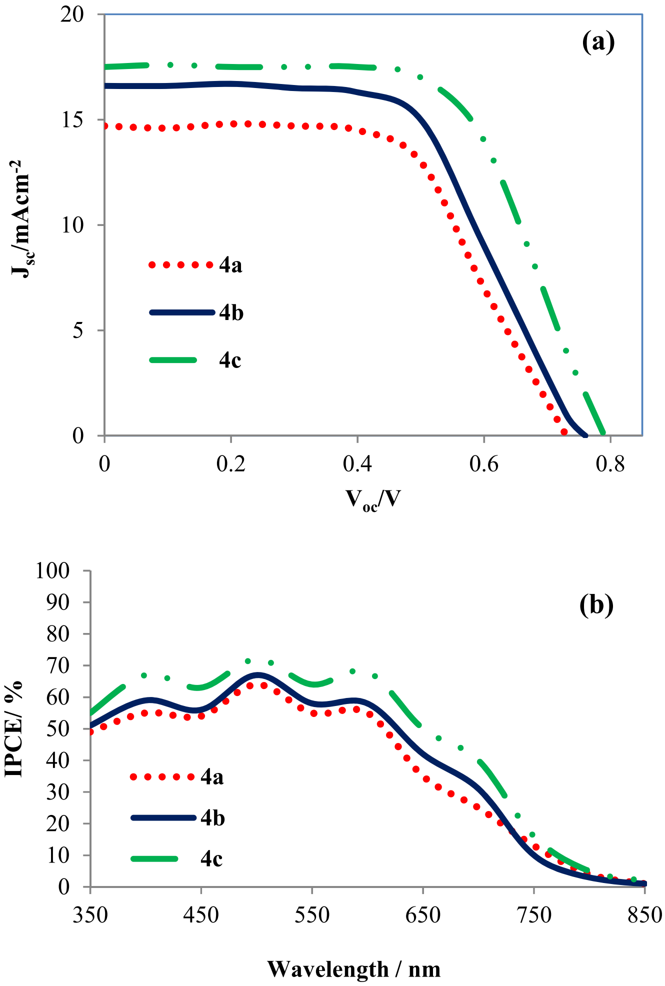

Fig. 9. (a) I–V curves, (b) IPCE spectra of dyes **4a**–**c**.

Table 9
Photovoltaic parameters of dyes **4a**–**c.**

Dye	J_{SC} (mA.cm^{-2})	V_{OC} (V)	*FF* (%)	*η* (%)
4a	14.92	0.73	64	6.95
4b	16.62	0.76	71	7.06
4c	17.60	0.79	73	7.18

photovoltaic performance in the dyes, a great attempt to functionalization of the dyes is in progress and will soon be published elsewhere.

Acknowledgment

We would like to express our sincere gratitude to Research Office, Mashhad Branch, Islamic Azad University, Mashhad-Iran, for financial support of this work.

References

[1] T. Maeda, T.V. Nguyen, Y. Kuwano, X. Chen, K. Miyanaga, H. Nakazumi, S. Yagi, S. Soman, A. Ajayaghosh, Intramolecular exciton-coupled squaraine dyes for dye-sensitized solar cells, J. Phys. Chem. C 122 (38) (2018 Sep 5) 21745–21754.

[2] M. Urbani, M.E. Ragoussi, M.K. Nazeeruddin, T. Torres, Phthalocyanines for dye-sensitized solar cells, Coord. Chem. Rev. 381 (2019 Feb 15) 1–64.

[3] T. Higashino, H. Imahori, Porphyrins as excellent dyes for dye-sensitized solar cells: recent developments and insights, Dalton Trans. 44 (2) (2015) 448–463.

[4] K.S. Reddy, Y.C. Chen, C.C. Wu, C.W. Hsu, Y.C. Chang, C.M. Chen, C.Y. Yeh, Cosensitization of structurally simple porphyrin and anthracene-based dye for dye-sensitized solar cells, ACS Appl. Mater. Interfaces 10 (3) (2018 Jan 10) 2391–2399.

[5] Y. Cui, W. Zhao, S. Ogasawara, X.F. Wang, H. Tamiaki, Fabrication and performance of all-solid-state dye-sensitized solar cells using synthetic carboxylated and pyridylated chlorophyll derivatives, J. Photochem. Photobiol. A Chem. 353 (2018 Feb 15) 625–630.

[6] C.H. Siu, L.T. Lee, S.C. Yiu, P.Y. Ho, P. Zhou, C.L. Ho, T. Chen, J. Liu, K. Han, W.Y. Wong, Synthesis and characterization of phenothiazine-based platinum (II)–Acetylide photosensitizers for efficient dye-sensitized solar cells, Chem. A Eur. J. 22 (11) (2016 Mar 7) 3750–3757.

[7] P. Yang, J. Duan, D. Liu, Q. Tang, B. He, Multi-interfacial polyaniline-graphene/platinum counter electrodes for dye-sensitized solar cells, Electrochim. Acta 173 (2015 Aug 10) 331–337.

[8] M.S. Su'ait, M.Y. Rahman, A. Ahmad, Review on polymer electrolyte in dye-sensitized solar cells (DSSCs), Sol. Energy 115 (2015 May 1) 452–470.

[9] S.M. Lopes, E.P. Sousa, L. Barreira, C. Marques, M.J. Rodrigues, T.M. e Melo, Synthesis and anti-cancer activity of chiral tetrahydropyrazolo [1, 5-a] pyridine-fused steroids, Steroids 122 (2017 Jun 1) 16–23.

[10] C. Ravi, A. Qayum, D.C. Mohan, S.K. Singh, S. Adimurthy, Design, synthesis and cytotoxicity studies of novel pyrazolo [1, 5-a] pyridine derivatives, Eur. J. Med. Chem. 126 (2017 Jan 27) 277–285.

[11] A.S. Hassan, M.F. Mady, H.M. Awad, T.S. Hafez, Synthesis and antitumor activity of some new pyrazolo [1, 5-a] pyrimidines, Chin. Chem. Lett. 28 (2) (2017 Feb 1) 388–393.

[12] A.M. Fouda, H.A. Abbas, E.H. Ahmed, A.A. Shati, M.Y. Alfaifi, S.E. Elbehairi, Synthesis, in vitro antimicrobial and cytotoxic activities of some new pyrazolo [1, 5-a] pyrimidine derivatives, Molecules 24 (6) (2019 Jan) 1080.

[13] K. Ochiai, N. Ando, K. Iwase, T. Kishi, K. Fukuchi, A. Ohinata, H. Zushi, T. Yasue, D.R. Adams, Y. Kohno, Phosphodiesterase inhibitors. Part 2: design, synthesis, and structure–activity relationships of dual PDE3/4-inhibitory pyrazolo [1, 5-a] pyridines with anti-inflammatory and bronchodilatory activity, Bioorg. Med. Chem. Lett 21 (18) (2011 Sep 15) 5451–5456.

[14] L.W. Zheng, J.H. Shao, B.X. Zhao, J.Y. Miao, Synthesis of novel pyrazolo [1, 5-a] pyrazin-4 (5H)-one derivatives and their inhibition against growth of A549 and H322 lung cancer cells, Bioorg. Med. Chem. Lett 21 (13) (2011 Jul 1) 3909–3913.

[15] M.G. Mamolo, D. Zampieri, V. Falagiani, L. Vio, M. Fermeglia, M. Ferrone, S. Pricl, E. Banfi, G. Scialino, Antifungal and antimycobacterial activity of new N1-[1-aryl-2-(1Himidazol-1-yl and 1H-1, 2, 4-triazol-1-yl)-ethylidene]-pyridine-2-carboxamidrazone derivatives: a combined experimental and computational approach, Arkivoc 231 (2004 Jan 1) 250.

[16] X. Lu, J. Tang, S. Cui, B. Wan, S.G. Franzblauc, T. Zhang, X. Zhang, K. Ding, Pyrazolo [1, 5-a] pyridine-3-carboxamide hybrids: design, synthesis and evaluation of anti-tubercular activity, Eur. J. Med. Chem. 125 (2017 Jan 5) 41–48.

[17] R. Ducray, P. Boutron, M. Didelot, H. Germain, F. Lach, M. Lamorlette, A. Legriffon, M. Maudet, M. Ménard, G. Pasquet, F. Renaud, A versatile route to 3-(pyrimidin-4-yl)-imidazo [1, 2-a] pyridines and 3-(pyrimidin-4-yl)-

Please cite this article as: Z. Agheli et al., Synthesis, characterization, optical properties, computational characterizations, QTAIM analysis and cyclic voltammetry of new organic dyes for dye-sensitized solar cells, Journal of Molecular Structure, https://doi.org/10.1016/j.molstruc.2019.127228

pyrazolo [1, 5-a] pyridines, Tetrahedron Lett. 51 (36) (2010 Sep 8) 4755–4758.
[18] P. Yan, G. Duan, R. Ji, Y. Ge, A simple and efficient synthesis of new fluorophore 4-hydroxy pyrazolo [1, 5-a] pyridines through a tandem reaction, Tetrahedron Lett. 59 (25) (2018 Jun 20) 2426–2429.
[19] P. Zhang, H. Lv, G. Duan, J. Dong, Y. Ge, A novel pyrazolo [1, 5-a] pyridine fluorophore and its application to detect pH in cells, RSC Adv. 8 (54) (2018) 30732–30735.
[20] A. Tigreros, H.A. Rosero, J.C. Castillo, J. Portilla, Integrated pyrazolo [1, 5-a] pyrimidine–hemicyanine system as a colorimetric and fluorometric chemosensor for cyanide recognition in water, Talanta 196 (2019 May 1) 395–401.
[21] V. Boekelheide, N.A. Fedoruk, Syntheses of fused aromatic heterocycles by 1, 3-dipolar addition reactions. 3-Azapyrrocolines, J. Org. Chem. 33 (5) (1968 May) 2062–2064.
[22] K.I. Tanji, T. Sasahara, J. Suzuki, T. Higashino, Pyrazolopyridines. I: formylation and acylation of pyrazolo [1, 5-a] pyridines, Heterocycles 35 (2) (1993) 915–924.
[23] E. Lammers, J. Nusstein, A. Reader, M. Drum, M. Beck, S. Fowler, Does the combination of 3% mepivacaine plain plus 2% lidocaine with epinephrine improve anesthesia and reduce the pain of anesthetic injection for the inferior alveolar nerve block? A prospective, randomized, double-blind study, J. Endod. 40 (9) (2014 Sep 1) 1287–1292.
[24] J.E. Peralta, G.E. Scuseria, M.J. Frisch, Noncollinear magnetism in density functional calculations, Phys. Rev. B 75 (12) (2007 Mar 27) 125119.
[25] D.C. Young, Computational Drug Design: a Guide for Computational and Medicinal Chemists, John Wiley & Sons, 2009 Jan 28.
[26] R. Ditchfield, Self-consistent perturbation theory of diamagnetism: I. A gauge-invariant LCAO method for NMR chemical shifts, Mol. Phys. 27 (4) (1974 Apr 1) 789–807.
[27] G. Zhurko, D. Zhurko, Chemcraft, Version 1.7 (build 365), 2013, http://www.chemcraftprog.com. (Accessed 27 March 2016).
[28] T.A. Keith, AIMAll (Version 13.11. 04), TK Gristmill Software, Overland Park KS, USA, 2013.
[29] R.F. Bader, A quantum theory of molecular structure and its applications, Chem. Rev. 91 (5) (1991 Jul 1) 893–928.
[30] N.N. Dinh, N.M. Quyen, L. Ha Chi, T.T. Thuy, T.Q. Trung, Characterization of solar cells using nano titanium oxide and nanocomposite materials, in: AIP Conference Proceedings vol. 1169, AIP, 2009 Sep 14, pp. 25–31. No. 1.
[31] M.R. Rodríguez, J. Del Plá, O.E. Piro, G.A. Echeverría, G. Espino, R. Pis-Diez, B.S. Parajón-Costa, A.C. González-Baró, Structure, tautomerism, spectroscopic and DFT study of o-vanillin derived Schiff bases containing thiophene ring, J. Mol. Struct. 1165 (2018 Aug 5) 381–390.
[32] V.P. Radha, S.J. Kirubavathy, S. Chitra, Synthesis, characterization and biological investigations of novel Schiff base ligands containing imidazoline moiety and their Co (II) and Cu (II) complexes, J. Mol. Struct. 1165 (2018 Aug 5) 246–258.
[33] F. Jafari-Moghaddam, S.A. Beyramabadi, M. Khashi, A. Morsali, Three VO2+ complexes of the pyridoxal-derived Schiff bases: synthesis, experimental and theoretical characterizations, and catalytic activity in a cyclocondensation reaction, J. Mol. Struct. 1153 (2018 Feb 5) 149–156.
[34] T. Toozandejani, S.A. Beyramabadi, H. Chegini, M. Khashi, A. Morsali, M. Pordel, Synthesis, experimental and theoretical characterization of a Mn (II) complex of N, N′-dipyridoxyl (1, 2-diaminobenzene), J. Mol. Struct. 1127 (2017 Jan 5) 15–22.
[35] H. Jouypazadeh, H. Farrokhpour, DFT and TD-DFT study of the adsorption and detection of sulfur mustard chemical warfare agent by the C24, C12Si12, Al12N12, Al12P12, Be12O12, B12N12 and Mg12O12 nanocages, J. Mol. Struct. 1164 (2018 Jul 15) 227–238.
[36] S. Samiee, S. Taghvaeian, The role of metals and dithiolate ligands on structural, electronic and optical properties of [M (bipyridine)(dithiolate)] complexes: a theoretical study, Spectrochim. Acta A Mol. Biomol. Spectrosc. 198 (2018 Jun 5) 150–159.
[37] M. Snehalatha, C. Ravikumar, I.H. Joe, N. Sekar, V.S. Jayakumar, Spectroscopic analysis and DFT calculations of a food additive Carmoisine, Spectrochim. Acta A Mol. Biomol. Spectrosc. 72 (3) (2009 Apr 1) 654–662.
[38] I. Rozas, I. Alkorta, J. Elguero, Behavior of ylides containing N, O, and C atoms as hydrogen bond acceptors, J. Am. Chem. Soc. 122 (45) (2000 Nov 15) 11154–11161.
[39] E. Espinosa, M. Souhassou, H. Lachekar, C. Lecomte, Topological analysis of the electron density in hydrogen bonds, Acta Crystallogr. Sect. B Struct. Sci. 55 (4) (1999 Aug 1) 563–572.
[40] S. Sasaki, G.P. Drummen, G.I. Konishi, Recent advances in twisted intramolecular charge transfer (TICT) fluorescence and related phenomena in materials chemistry, J. Mater. Chem. C 4 (14) (2016) 2731–2743.
[41] N.R. Chowdhury, R. Kant, Theory of generalized Gerischer impedance for quasi-reversible charge transfer at rough and finite fractal electrodes, Electrochim. Acta 281 (2018 Aug 10) 445–458.

Please cite this article as: Z. Agheli et al., Synthesis, characterization, optical properties, computational characterizations, QTAIM analysis and cyclic voltammetry of new organic dyes for dye-sensitized solar cells, Journal of Molecular Structure, https://doi.org/10.1016/j.molstruc.2019.127228